DALTON
FULL PAPER

Partial frustration of magnetic order in synthetic angelellite, $Fe_4As_2O_{11}$ †

Jon P. Wright, Abbie C. McLaughlin and J. Paul Attfield *

Department of Chemistry, University of Cambridge, Lensfield Road, Cambridge, UK CB2 1EW. E-mail: jpa14@cam.ac.uk

Received 4th July 2000, Accepted 29th August 2000
First published as an Advance Article on the web 28th September 2000

The antiferromagnetic structure of $Fe_4As_2O_{11}$ has been solved from neutron powder diffraction data below the Neel temperature of 159 K. A $2a \times b \times c$ magnetic supercell is adopted and the two crystallographically distinct Fe^{3+} sites order with different critical exponents and with saturated magnetic moments of 3.34(2) and 4.37(2) μ_B. The large difference between these magnetic moments reflects differing degrees of frustration at the two sites. Structural refinement using high resolution powder neutron diffraction data confirms the structural model previously reported and no evidence for the presence of an OH group associated with a very short Fe–O distance of 1.76(2) Å is found.

Introduction

The relatively simple chemical formula of angelellite, $Fe_4As_2O_{11}$, hides a complex crystal chemistry. The crystal structure[1] of angelellite is triclinic (space group $P\bar{1}$) with two inequivalent octahedral iron sites in the asymmetric unit and a single tetrahedral arsenate anion. The structure contains an unusual oxide site which is co-ordinated only to two Fe^{3+} cations, resulting in a very short Fe–O distance of 1.772 Å. This short distance is in keeping with a regression analysis[2] and with bond valence sums for Fe^{3+}–O^{2-} bonds. Burdett *et al.*[3] discuss why such a complex crystal structure should arise for this compound. It is shown that there is no way of arranging octahedral Fe^{3+} and tetrahedral As^{5+} with O^{2-} anions to give all of the anions equivalent bond valence sums. This inevitably leads to a lower symmetry structure since some of the oxide anions must be inequivalent.

Expressing the chemical formula as $2Fe_2O_3{\cdot}As_2O_5$ suggests there may be similarities to hematite, Fe_2O_3, and indeed intergrowths of angelellite and hematite have been observed[4] in naturally occurring samples. Both structures are based on cubic close packing of the oxide anion lattice. The chemical formula may also be written as $Fe_4(O)O_2(AsO_4)_2$ to reflect the crystal structure, and Moore and Araki[1] suggested that a continuous solid solution may exist with $Fe_4(OH)O_2(AsO_4)_2$. The presence of the OH^- group was suggested in order to explain the undersaturation of the oxide involved in the short Fe–O bond. Evidence that the extra proton may not be essential to stabilise this structure type is provided by a study[5] of the Fe_2O_3–As_2O_5 phase diagram which shows that anhydrous $FeAsO_4$ decomposes upon heating to give an angelellite phase.

Our continuing studies of magnetic superexchange mechanisms across tetrahedral anions[6,7] led us to consider this compound. The unusually short, linear Fe–O–Fe linkage gives a part of the structure where the exchange interaction may reliably be predicted to be strongly antiferromagnetic, so that the remaining interactions can be inferred more easily. Magnetic susceptibility measurements and neutron diffraction experiments have been carried out in order to probe the magnetic properties of this structure. The magnetic structure has been solved from a variable temperature neutron diffraction study and high resolution neutron diffraction data were collected to investigate the possible presence of the additional proton.

† Dedicated to the memory of Ron Snaith, friend, colleague and teacher.

Experimental

The production of synthetic samples of angelellite has been discussed in detail by Berdesinski.[8] 29.9433 g $Fe(NO_3)_3{\cdot}9H_2O$ and 5.1652 g $As_2O_5{\cdot}xH_2O$ ($x \approx 3$) were dissolved in 2 M HNO_3 and the resulting solution was boiled to dryness. The residue was ground using an agate pestle and mortar and heated to 700 °C for 12 hours. X-Ray powder diffraction measurements indicated the major product was $Fe_4As_2O_{11}$ with an $FeAsO_4$ impurity phase. No other impurity phases were detected and a Rietveld refinement was carried out from which the phase fraction of $FeAsO_4$ was estimated as 9.5(7) wt.%.

Variable temperature neutron diffraction data were collected at the Institute Laue Langevin, Grenoble, France, using the D20 diffractometer. Data were collected at intervals of 2 K between 2 and 300 K with an incident neutron wavelength of 2.41 Å. The D20 data were fitted using the PRODD computer program.[9] Further data were collected at the ISIS Facility, Didcot, UK, using the OSIRIS[10] instrument, at a temperature of 200 K. The OSIRIS data were fitted using the GSAS[11] suite of computer programs.

Magnetic susceptibility data were collected between 10 and 300 K from a 27.8 mg sample in a Quantum Design SQUID magnetometer. The sample was cooled in zero field then warmed in the measuring field of 1.0 T.

Results

Fig. 1 shows the variable temperature neutron diffraction data, where the appearance of peaks due to magnetic ordering in the two phases is clearly evident. The magnetic structure of $FeAsO_4$ is known and hence magnetic peaks due to angelellite could be assigned unambiguously. All of these magnetic peaks could be indexed as (h/2 k l) showing that the magnetic unit cell has the a axis doubled compared to that of the nuclear cell. The evolutions of two selected peaks with temperature is indicated in the inset to Fig. 1 from which it is clear that the variations are not the same. This shows that the magnetic structure must have two or more degrees of freedom that do not follow the same temperature dependence.

Solution of the magnetic structure was achieved by considering starting models in magnetic space groups $P\bar{1}$ and $P\bar{1}'$. There are two inequivalent iron sites in the asymmetric unit and moments were placed parallel and anti-parallel on

DOI: 10.1039/b005350n

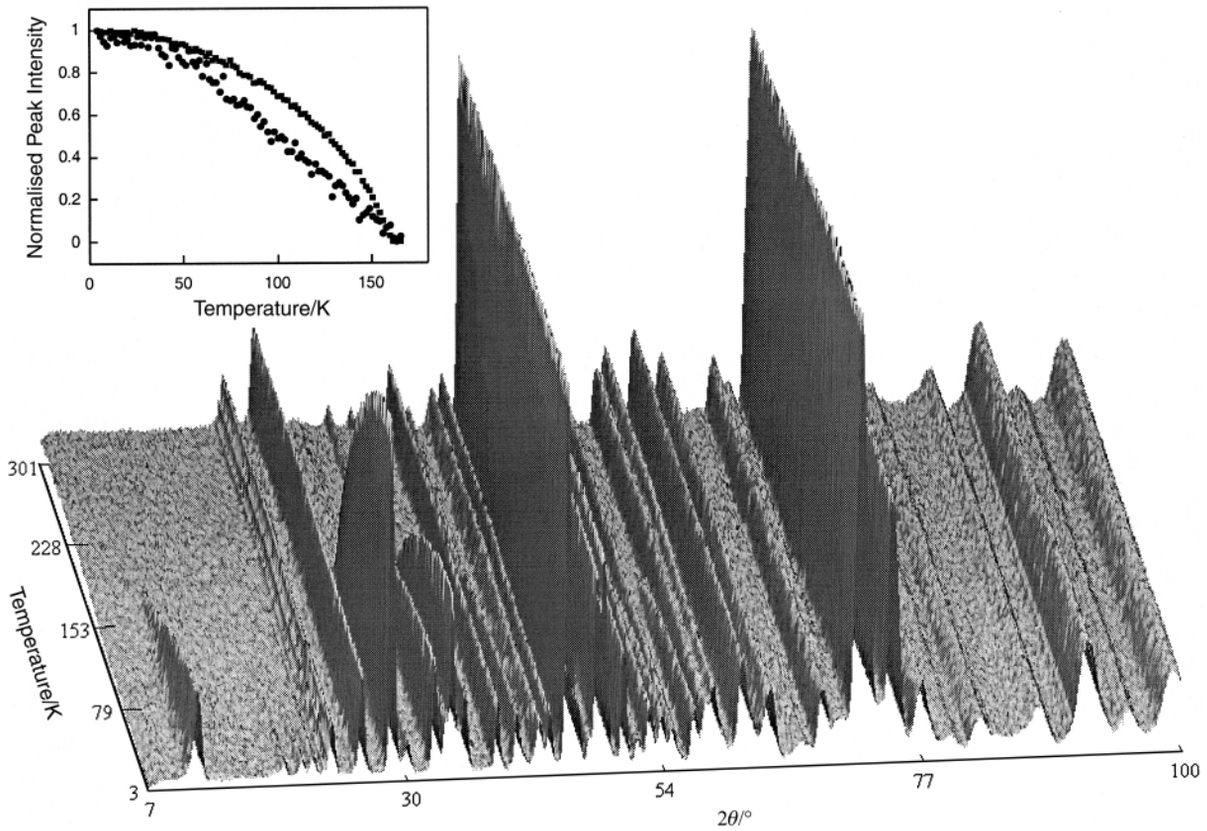

Fig. 1 Neutron diffraction patterns of $Fe_4As_2O_{11}$ from D20 plotted as a function of temperature. Inset shows the evolution of the (1/2 0 0) (circles) and the (1/2 0 $\bar{1}$) (squares) magnetic peaks at 11.4 and 29.0° respectively.

Table 1 Models for the magnetic structure in $Fe_4As_2O_{11}$ at 2 K. In all cases the moment directions were perpendicular to a, making an angle φ to c^*. χ^2 is the goodness of fit to the powder diffraction pattern

Model	Fe1 moment/μ_B	Fe2 moment/μ_B	Fe1 φ/°	Fe2 φ/°	χ^2
1	3.85(3)	=Fe1	97.2(9)	=Fe1	11.65
2	3.86(2)	=Fe1	84.4(7)	107.7(7)	6.46
3	3.34(2)	4.37(2)	96.9(6)	=Fe1	5.24
4	3.35(3)	4.26(2)	96(2)	97(1)	5.25

these sites, in each of the magnetic space groups. Atomic coordinates from ref. 1 were used for all fits to the D20 data. Refinement of the moment magnitude and directions for the best model found by this procedure (model 1 in Table 1) led to a fairly good overall fit. However, the calculated intensity of the (1/2 0 0) magnetic peak at $2\theta = 11.4°$ was too small. No other model with equivalent magnitudes and directions for moments on the two iron sites was able to produce a comparable fit.

Refinement of the magnetic structure proceeded by relaxing the constraints between the two iron sites such that the magnitude and directions of the moments were allowed to differ for each site. The fit to the (1/2 0 0) intensity was much improved and the refinement converged with significantly different magnitudes, but similar directions for the magnetic moments (model 4). Further investigations of models where the directions were constrained to be equivalent (model 3), but the magnitudes were allowed to differ, produced no statistically significant degradation in fit. However, constraining the magnitudes of the moments and allowing the directions to refine produced a poorer fit (model 2). Model 3 was thus taken to be the correct magnetic structure. A summary of the refined models is given in Table 1.

Model 3 was fitted to all of the datasets where magnetic peaks were visible in order to extract the temperature dependence of the parameters. $FeAsO_4$ was fitted as an impurity phase using the model described previously for the subset of data below 84 K. Fig. 2 shows the fit to the 2 K dataset. The thermal variations of the refined magnetic moments are shown in Fig. 3 and a graphical depiction of the magnetic structure is in Fig. 4. The $Fe_4As_2O_{11}$ moments $\mu(T)$ were fitted by the critical expression (1) for 107 K ($0.67\ T_N$) < T < T_N. The fitted values

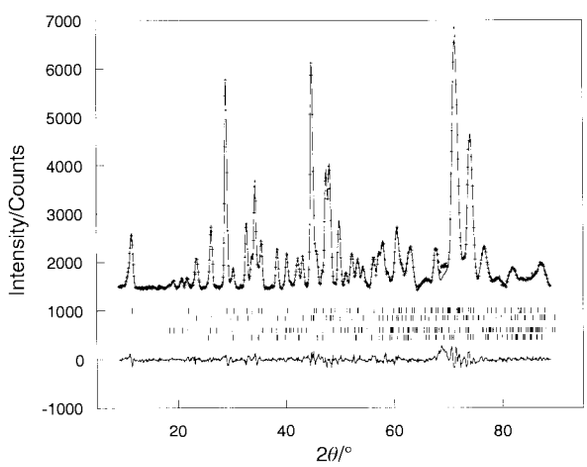

Fig. 2 Rietveld plot for the 2 K D20 dataset. Crosses: observed data. Lines: calculated and difference. Reflection position markers: upper row, $Fe_4As_2O_{11}$ magnetic peaks; upper middle, $Fe_4As_2O_{11}$ nuclear peaks; lower middle, $FeAsO_4$ magnetic peaks; lower row, $FeAsO_4$ nuclear peaks.

$$\mu(T) = \mu_0[1 - (T/T_N)]^{\beta} \quad (1)$$

of the critical exponent β were 0.316(9) and 0.360(7) for the Fe1 and Fe2 sites and the corresponding values of T_N were 157.9(3) and 159.4(3) K. Both β values are close to the calculated value of 0.345 for a three dimensional Heisenberg magnet.[12]

Fig. 5 shows the variation of the six cell parameters with temperature, as obtained from the D20 data. A minimum in the a parameter and a change in slope for the angle β are found around T_N.

Rietveld analysis of the OSIRIS data using the coordinates reported from a single crystal X-ray experiment quickly led to a good fit. With the neutron scattering lengths of Fe, O, As and H being 9.45, 5.803, 6.58 and −3.74 fm respectively, the presence of an OH^- group in the structure should easily be confirmed. Refinement of the atomic positions led to the structural model summarised in Table 2. The resulting F_{hkl} map did not contain any peaks near the undersaturated oxide, nor is there the large incoherent background scattering that would be observed if H were present.

The atomic positions are essentially in agreement with those previously reported. The quality of the refinement is slightly poorer, as judged on the basis of the esds. This is due to the overlap of peaks in the powder method and the more limited range of reciprocal space examined. However, neutron diffraction is much more sensitive to the presence of hydrogen and these data show no evidence to suggest that hydrogen is present in this sample. Fig. 6 shows the Rietveld fit for the OSIRIS data.

Fig. 7 shows the magnetisation data obtained from the SQUID experiments. The data above 200 K were fitted by the Curie–Weiss law leading to values of 5.82(3) μ_B for the paramagnetic moment (averaged over 90% $Fe_4As_2O_{11}$ and 10% $FeAsO_4$) and −553(9) K for the average Weiss temperature. The data show a maximum at 152(2) K, which corresponds to T_N.

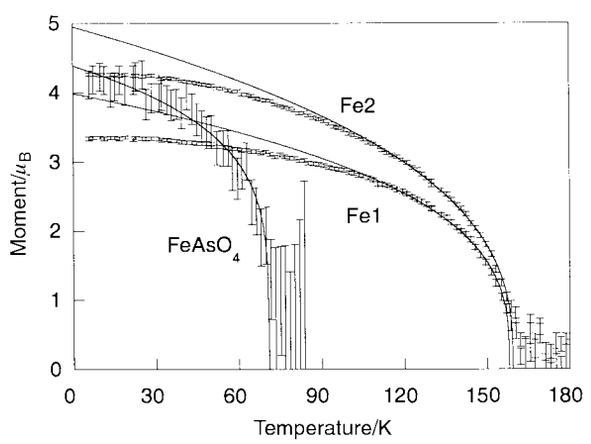

Fig. 3 Refined magnetic moments for the two iron sites in $Fe_4As_2O_{11}$ and for the $FeAsO_4$ secondary phase as a function of temperature.

The broad shoulder at 60–100 K is due to the magnetic ordering in $FeAsO_4$.[13]

Discussion

The crystal structure of angelellite refined here is essentially in agreement with that previously reported. The unusually short Fe^{3+}–O distance of 1.76 Å (Table 3) is reproduced and we find no evidence for the presence of an additional hydrogen atom. Preparation of a sample of $Fe_4As_2O_{10}(OH)$ would be of considerable interest as this may modify the dominant superexchange interaction present in this system. The crystal structure is illustrated in Fig. 8; it consists of chains of edge sharing

Table 2 Structural results from refinement of $Fe_4As_2O_{11}$ in space group $P\bar{1}$ using OSIRIS neutron data collected at 200 K

Atom	x	y	z
Fe1	0.7575(3)	0.0282(3)	0.0963(4)
Fe2	0.3746(3)	0.7467(3)	0.3448(4)
As	0.8151(4)	0.6073(4)	0.3360(6)
O1	0.6552(5)	0.7344(5)	0.2104(6)
O2	0.0907(5)	0.7903(5)	0.4615(6)
O3	0.7268(5)	0.5433(5)	0.6050(6)
O4	0.7927(5)	0.3725(6)	0.0782(7)
O5	0	0	0
O6	0.4685(4)	0.0423(5)	0.2605(7)

Agreement factors: $\chi^2 = 6.44$, $R_{Bragg} = 7.3\%$, $R_p = 1.2\%$ and $R_{wp} = 1.5\%$. Cell parameters: $a = 6.47365(7)$, $b = 6.59962(8)$, $c = 5.03760(7)$ Å, $\alpha = 106.2501(9)$, $\beta = 89.4384(11)$, $\gamma = 108.7519(21)°$, $V = 188.910(4)$ Å^3. Overall isotropic thermal factor = 0.0124(4) Å^2.

Table 3 Selected bond distances (Å) and angles (°) for $Fe_4As_2O_{11}$ at 200 K

Fe1–O1	2.107(3)	Fe2–O3	1.915(3)
Fe1–O2	2.114(3)	Fe2–O4	2.042(3)
Fe1–O4	2.239(3)	Fe2–O6	2.033(3)
Fe1–O5	1.760(2)	Fe2–O6	1.968(3)
Fe1–O6	2.171(3)	As–O1	1.685(3)
Fe1–O6	1.977(3)	As–O2	1.703(3)
Fe2–O1	2.047(3)	As–O3	1.654(3)
Fe2–O2	2.090(3)	As–O4	1.668(3)
Fe1–O1–Fe2	101.96(15)	Fe1–O6–Fe2	100.21(12)
Fe1–O2–Fe2	97.85(14)	Fe1–O6–Fe2	99.83(14)
Fe1–O4–Fe2	95.03(15)	Fe1–O6–Fe2	103.98(16)
Fe1–O5–Fe1	180.0	Fe1–O6–Fe2	146.54(14)
Fe1–O6–Fe1	100.86(15)	Fe2–O6–Fe2	97.85(15)

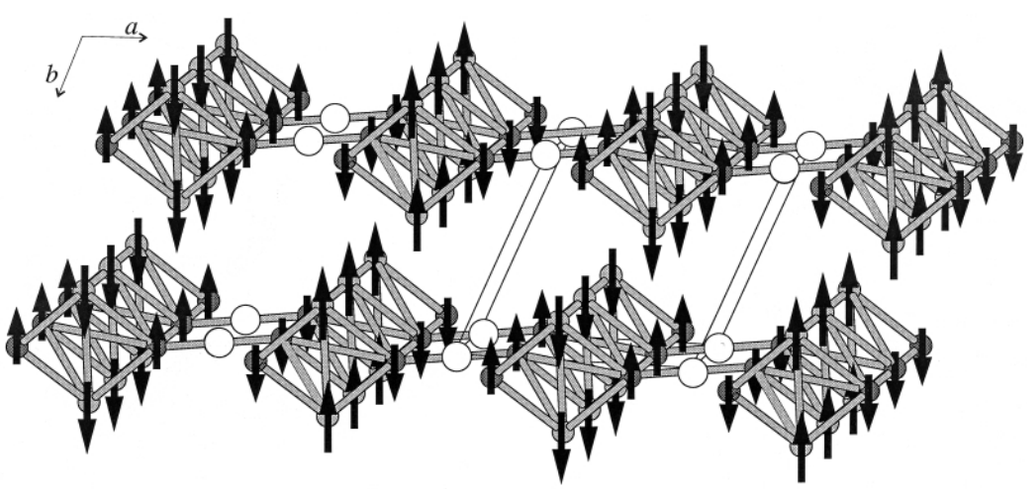

Fig. 4 Graphical illustration of the magnetic structure in $Fe_4As_2O_{11}$. For clarity the tetrahedral arsenate groups are omitted. Bonds indicate connections between edge sharing iron octahedra. Dark grey, Fe1; light grey, Fe2; open circles are the two-co-ordinate oxide anions. The nuclear cell is shown.

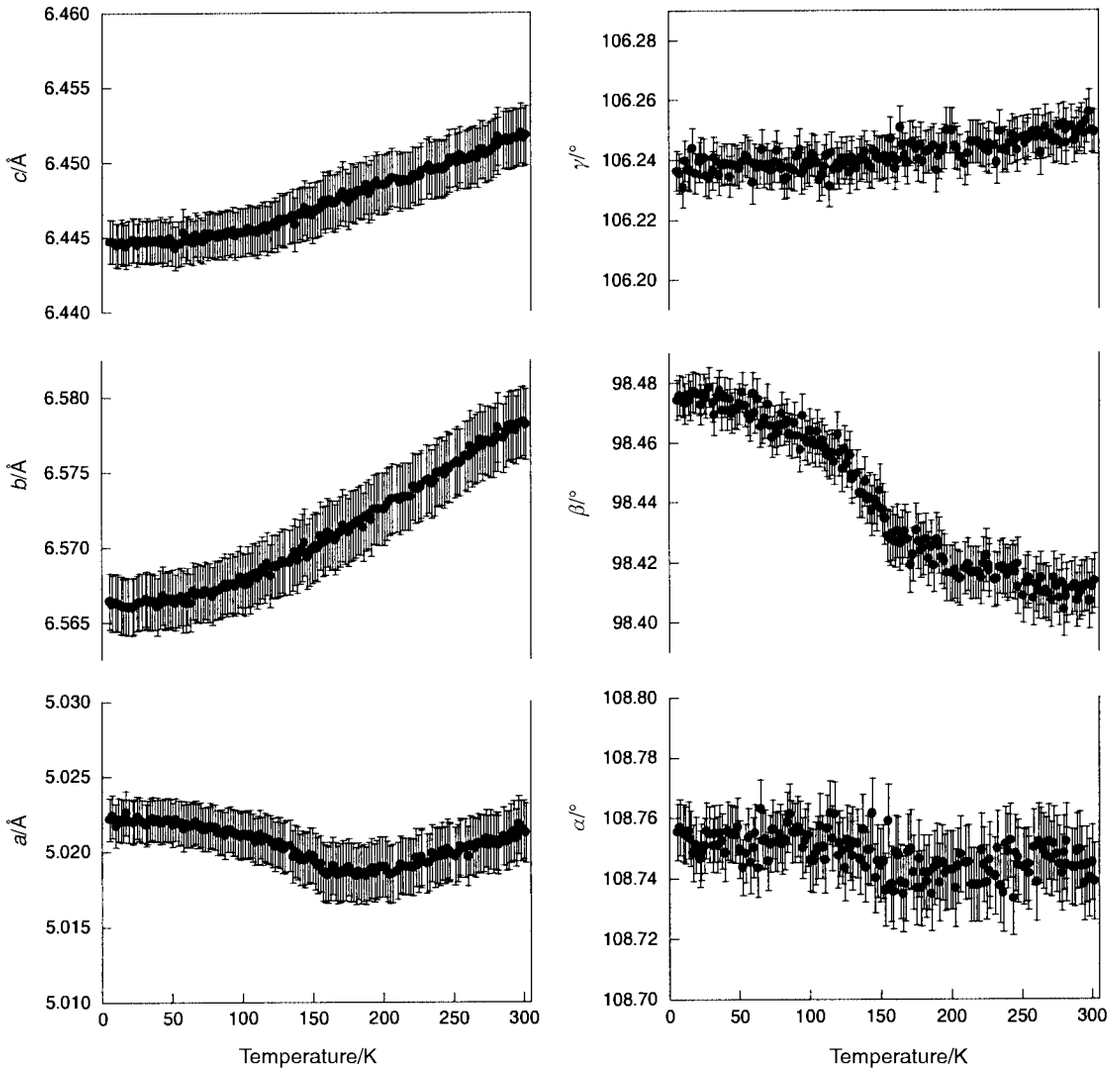

Fig. 5 Refined cell parameters for $Fe_4As_2O_{11}$ *versus* temperature from the D20 data.

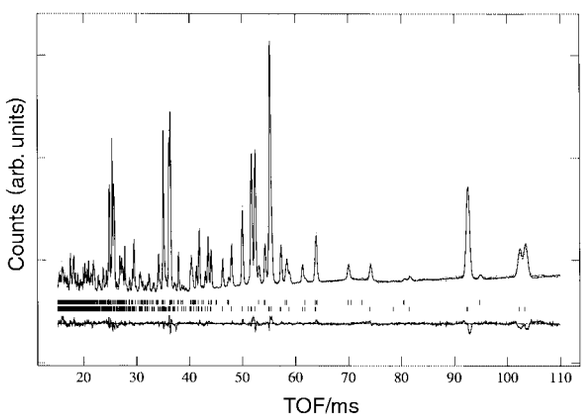

Fig. 6 Rietveld plot for the 200 K OSIRIS data; upper tick marks, $FeAsO_4$; lower tick marks, $Fe_4As_2O_{11}$. The time-of-flight (TOF) range corresponds to $d = 0.86$–6.3 Å.

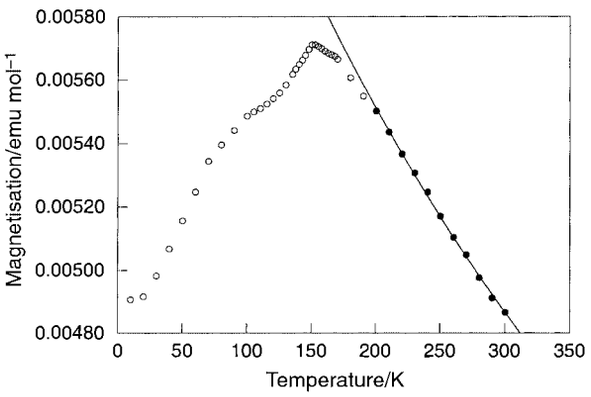

Fig. 7 Magnetic susceptibility data for $Fe_4As_2O_{11}$. Filled circles indicate those points fitted with the Curie–Weiss curve (solid line).

octahedra forming a spiral in the *c* direction. These are linked by corners to form infinite sheets, perpendicular to *b*, separated by arsenate tetrahedra.

Angelellite is unusual in having two chemically similar Fe^{3+} cations with markedly different saturated magnetic moments. The explanation for this observation must be based on the differences between the geometries around the two cation sites. Spontaneous static ordering of magnetic moments at low temperatures is caused by exchange interactions between the moments, making it energetically favourable for them to align either parallel or anti-parallel. In insulating oxides there are two principal mechanisms by which magnetic exchange is mediated; superexchange and direct exchange. The latter is a direct interaction between the magnetic moments that results from overlap of the cation d orbitals. Goodenough[14] has shown that there is a critical minimum distance for significant d-orbital overlap to occur. This distance is 2.58 Å in the case of Fe^{3+}, which is significantly less than the Fe···Fe distances in angelellite which are 3.20, 3.16 and 3.02 Å. Therefore direct exchange between the edge sharing octahedra can be ruled out as an exchange mechanism here.

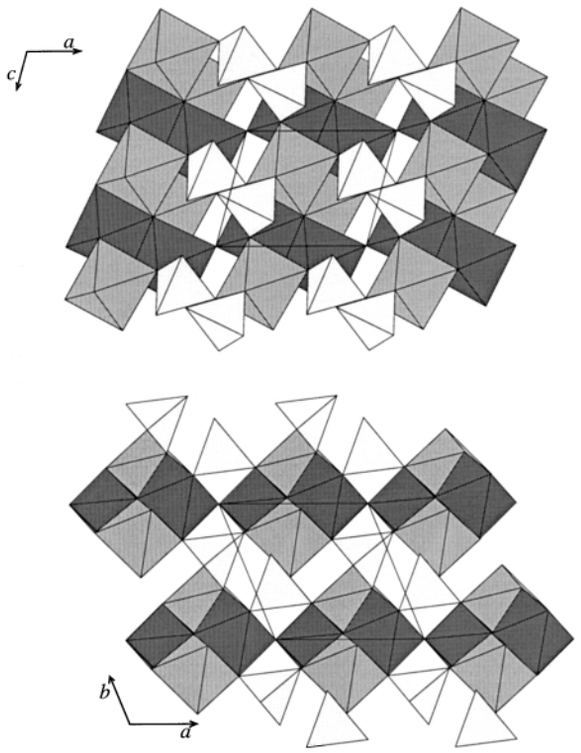

Fig. 8 Crystal structure of $Fe_4As_2O_{11}$. Above: projection on the *ac* plane, looking down on an Fe–O sheet. Below: projection on the *ab* plane. Dark grey octahedra, Fe1; mid-grey octahedra, Fe2; light grey tetrahedra, As.

Superexchange interactions are well understood for a simple cation–anion–cation pathway. The interaction is strongly antiferromagnetic for a linear 180° Fe–O–Fe bond angle, but weakly ferromagnetic for an angle of 90°, with the crossover at around 96°. Thus we expect the linear Fe1–O5–Fe1 interaction to be strongly antiferromagnetic and the moments are indeed ordered in this way in the structure (Fig. 4). All other Fe–O–Fe linkages in the structure are *via* edge sharing octahedra with bond angles ranging from 95 to 146.5° (Table 3). Therefore, we expect all interactions between edge sharing octahedra to be antiferromagnetic, or nearly zero, with different strengths of interaction for each of the pathways.

The "bonds" illustrated in Fig. 4 show the paths of these exchange interactions within the structure. It is immediately clear that the cations are arranged tetrahedrally with respect to each other. This leads to a frustrated structure, as there is no way of placing four magnetic moments on the vertices of a tetrahedron with all edges linking anti-parallel moments. The strongest of the edge sharing interactions should be that corresponding to the 146.5° Fe1–O6–Fe2 linkage. Hence, we expect to find that the Fe1 moments will be anti-parallel to those on one of the Fe2 sites. The Fe1–O–Fe1 bond angle within the chain of edge-sharing octahedra is 100.8°, which is slightly lower than that for the other Fe1–O–Fe2 pathway. Thus, the arrangement of the magnetic moments within the infinite Fe–O layers is accounted for entirely by superexchange arguments. The Fe1 moments are anti-parallel to the Fe2 moments within a chain of edge-sharing octahedra, as these have pathways with the highest bond angles. The chains of octahedra are then arranged with moments anti-parallel to each other due to the strong linear superexchange interaction where the octahedra share a corner.

The degree of frustration at each of the iron sites will depend on the strength of the exchange interaction across the linkage where the moments are aligned parallel. In the case of the Fe2–O–Fe2 pathway the angle is 97.9°, compared to 100.8° for the Fe1–O–Fe1 pathway. This small difference in bond angle would predict that the Fe2–O–Fe2 would be less frustrated as the exchange interaction is more weakly antiferromagnetic. Hence, the Fe1 site order will be more frustrated than that at the Fe2 site, as observed. The refined value of the saturated moment for the Fe2 site (4.37(2) μ_B) is in agreement with the value of 5.0 μ_B expected for high spin Fe^{3+}, allowing for the usual ≈10% reduction due to covalency and zero point spin deviation. The value of 3.34(2) μ_B for Fe1 is further reduced by 1.0 μ_B due to the frustration at this site.

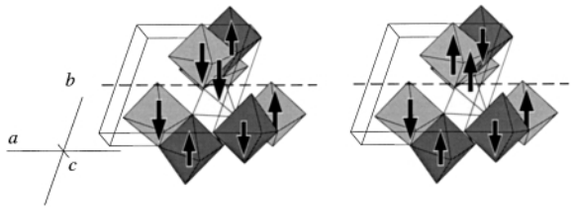

Fig. 9 The co-ordination of FeO_6 octahedra around a single arsenate anion. Alternative spin arrangements, assuming superexchange couplings within the Fe–O sheets are stronger than those across the anions, are shown. The arrangement on the left is observed experimentally. Colour scheme as for Fig. 7. Broken line indicates the separation between Fe–O sheets.

The refined cell parameters (Fig. 5) evidence a small exchange striction in this material. The response of the cell parameters to the magnetic transition is anisotropic and the largest changes are seen in the *a* parameter and β angle. This reflects the strength of the magnetic interactions in the iron oxide layers in the *ac* plane.

As alluded to in the introduction, one of the principal aims of this study was to examine the exchange interactions across the AsO_4^{3-} tetrahedron. Three of the four oxide anions involved in the tetrahedron are also part of the edge-sharing octahedra, the fourth being co-ordinated only to Fe2 and As. The observation from the magnetic structure is that the coupling between layers is ferromagnetic in the *b* direction. Each arsenate co-ordinates to four spins in one layer of octahedra and only three in the other. Assuming exchange through the arsenate anion is weaker than Fe–O–Fe interactions, these spins are fixed with respect to each other in each layer and the only remaining choice is the relative orientations of the spins in each layer. Fig. 9 illustrates the two possible arrangements and we observed that the one on the left is favoured in this material.

The high temperature paramagnetic moment of 5.82(3) μ_B for this $Fe_4As_2O_{11}$ sample is in good agreement with the prediction of the spin only formula for Fe^{3+} (μ_{so} = 5.92 μ_B). This value is averaged over the two iron sites in $Fe_4As_2O_{11}$ and the $FeAsO_4$ secondary phase. The susceptibility maximum at T_N = 152 K in a field of 1.0 T is in good agreement with the value of 159 K found in the zero field neutron diffraction experiment.

In summary, the magnetic structure of angelellite, $Fe_4As_2O_{11}$, has been determined. The arrangement of magnetic moments can be explained in terms of simple superexchange arguments with the exception of the interlayer coupling across the arsenate group. Two possible configurations are to be expected assuming the couplings within the layers are stronger, and one of these is adopted. Both iron spins order at the same temperature of 159 K although the critical exponents, β, differ significantly from each other due to frustration of magnetic order for one of the two sites.

Acknowledgements

We are grateful to EPSRC for provision of neutron beam time, Drs T. Hansen, A. Hewat and J. A. McAllister for assistance with the collection of D20 data, and Dr D. Martin for assistance with OSIRIS data collection. J. P. W. and A. C. M. acknowledge EPSRC for studentships and J. P. W. thanks the Rutherford Appleton Laboratory for CASE support.

References

1 P. B. Moore and T. Araki, *Neues Jahrb. Mineral.*, *Abh.*, 1978, **132**, 91.
2 W. H. Baur, *Trans. Am. Crystallogr. Assoc.*, 1970, **6**, 129.
3 J. K. Burdett, C. Marians and J. F. Mitchell, *Inorg. Chem.*, 1994, **33**, 1848.
4 K. Weber, *Neues Jahrb. Mineral.*, *Monatsh.*, 1959, 152.
5 B. K. Kasenov and E. S. Mustafin, *Zh. Neorg. Khim.*, 1997, **42**, 1746.
6 J. B. Forsyth, J. P. Wright, M. D. Marcos, J. P. Attfield and C. Wilkinson, *J. Phys.: Condens. Matter.*, 1999, **11**, 1473.
7 J. P. Wright, J. P. Attfield, W. I. F. David and J. B. Forsyth, *Phys. Rev. B*, 2000, **62**, 992; J. P. Wright, D. Martín y Marero and J. P. Attfield, *Physica B*, 2000, **276**–**278**, 682.
8 W. Berdesinski, *Neues Jahrb. Mineral.*, *Abh.*, 1960, **94**, 1203.
9 J. P. Wright and J. B. Forsyth, Rutherford Appleton Laboratory Report, RAL-TR-2000-012, 2000.
10 D. Martín y Marero, D. Engberg and K. H. Andersen, *Physica B*, 2000, **276**, 150.
11 A. C. Larson and R. B. Von Dreele, Los Alamos National Laboratory Report, Number LAUR 86-748, 1994.
12 H. Stanley, *Introduction to Phase Transitions and Critical Phenomena*, OUP, Oxford, 1971.
13 W. M. Reiff, M. J. Kwiecien, R. J. B. Jakeman, A. K. Cheetham and C. C. Torardi, *J. Solid State Chem.*, 1993, **107**, 401.
14 J. B. Goodenough, *Prog. Solid State Chem.*, 1970, **5.**